Biochemistry

pubs.acs.org/biochemistry Article

Hydride Transfer Catalyzed by Glycerol Phosphate Dehydrogenase: Recruitment of an Acidic Amino Acid Side Chain to Rescue a Damaged Enzyme

Rui He, Judith R. Cristobal, Naiji Jabin Gong, and John P. Richard*

Cite This: *Biochemistry* 2020, 59, 4856–4863 Read Online

ACCESS | Metrics & More | Article Recommendations | Supporting Information

ABSTRACT: K120 of glycerol 3-phosphate dehydrogenase (GPDH) lies close to the carbonyl group of the bound dihydroxyacetone phosphate (DHAP) dianion. pH rate (pH 4.6–9.0) profiles are reported for k_{cat} and $(k_{cat}/K_m)_{dianion}$ for wild type and K120A GPDH-catalyzed reduction of DHAP by NADH, and for (k_{cat}/K_dK_{am}) for activation of the variant-catalyzed reduction by $CH_3CH_2NH_3^+$, where K_{am} and K_d are apparent dissociation constants for $CH_3CH_2NH_3^+$ and DHAP, respectively. These profiles provide evidence that the K120 side chain cation, which is stabilized by an ion-pairing interaction with the D260 side chain, remains protonated between pH 4.6 and 9.0. The profiles for wild type and K120A variant GPDH show downward breaks at a similar pH value (7.6) that are attributed to protonation of the K204 side chain, which also lies close to the substrate carbonyl oxygen. The pH profiles for $(k_{cat}/K_m)_{dianion}$ and (k_{cat}/K_dK_{am}) for the K120A variant show that the monoprotonated form of the variant is activated for catalysis by $CH_3CH_2NH_3^+$ but has no detectable activity, compared to the diprotonated variant, for unactivated reduction of DHAP. The pH profile for k_{cat} shows that the monoprotonated K120A variant is active toward reduction of enzyme-bound DHAP, because of activation by a ligand-driven conformational change. Upward breaks in the pH profiles for k_{cat} and $(k_{cat}/K_m)_{dianion}$ for K120A GPDH are attributed to protonation of D260. These breaks are consistent with the functional replacement of K120 by D260, and a plasticity in the catalytic roles of the active site side chains.

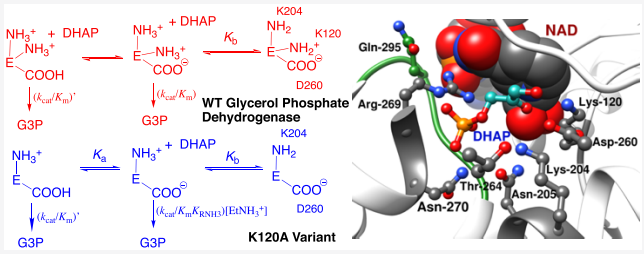

Glycerol 3-phosphate dehydrogenase (GPDH) catalyzes the reduction of dihydroxyacetone phosphate (DHAP) by NADH to form glycerol 3-phosphate [G3P (Scheme 1A)], a reaction that links the metabolism of glucose to form DHAP and the biosynthesis of phosphoglycerides from G3P.[1] Our interest in GPDH dates to the fortuitous observation that the activity of this enzyme for reduction of DHAP is largely retained during catalysis of the reduction of the substrate pieces glycolaldehyde and phosphite dianion (Scheme 1B),[2] and that the binding energy of the DHAP phosphodianion or the phosphite piece is utilized to transform the floppy inactive open form of GPDH into a stiff catalytically active protein cage.[3−6]

Scheme 1. (A) GPDH-Catalyzed Reaction of the Whole Substrate DHAP to Form Glycerol 3-Phosphate and (B) Phosphite Dianion Activation of GPDH for Catalysis for Reduction of the Substrate Piece Glycolaldehyde

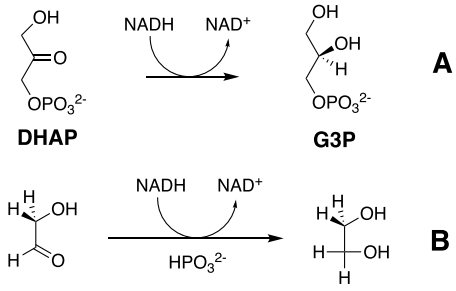

The structure of GPDH from human liver (*hl*GPDH) provides insight into the mechanism for enzyme-catalyzed hydride transfer from NADH to DHAP.[3,5] The following side chains line the enzyme active site (Figure 1)[7] and form a continuous chain of hydrogen bonds that stretch from the cofactor to the carbonyl group of DHAP: Q295, R269, N270, T264, N205, K204, D260, and K120.[5] Most of these side chains are completely conserved across 11 organisms; N205 and T264 are 91% conserved, while Q295 and E295 occur with nearly equal frequency.[7] Two of these side chains play a direct role in stabilizing the hydride transfer transition state. (1) The R269 side chain forms an ion pair with the substrate dianion.

Received: October 2, 2020
Revised: December 1, 2020
Published: December 11, 2020

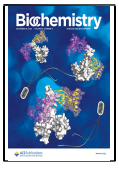

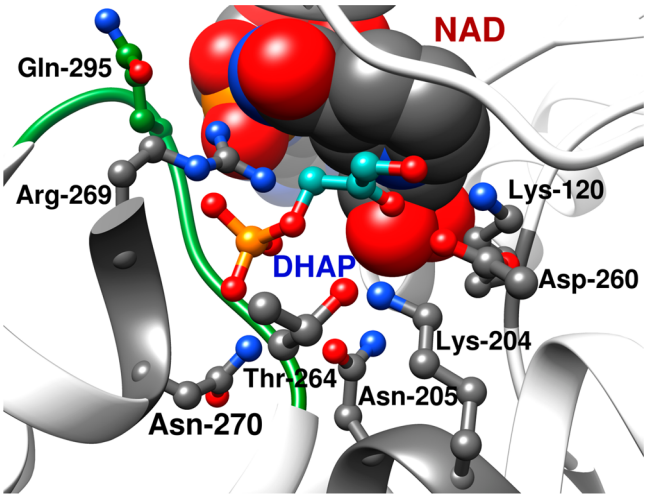

Figure 1. Representation of the X-ray crystal structure of the nonproductive E·NAD·DHAP complex of *hl*GPDH (Protein Data Bank entry 6E90). The following conserved amino acid side chains are shown: R269[8] and N270,[10] which interact with the substrate phosphodianion; Q295,[11] from a flexible enzyme loop that interacts with R269; K120 and K204,[5,9] which lie close to the carbonyl oxygen of DHAP; D260, which is ion-paired with K120;[5] and N205 and T264.

The R269A substitution results in a 10^5-fold decrease in k_{cat}/K_m for hydride transfer to DHAP.[8] (2) The K120 side chain cation is positioned to stabilize negative charge at the C-2 substrate oxygen of DHAP, which develops at the transition state for enzyme-catalyzed hydride transfer from NADH.[5] The K120A substitution results in a 10^4-fold decrease in k_{cat}/K_m for hydride transfer.[5,9]

The efficient rescue of the activity of the impaired K120A/R269A double variant by the combined action of ethylammonium and guanidinium cations[9] is consistent with a high degree of organization of the K120 and R269 side chains at the active site of *hl*GPDH. The K120 side chain is immobilized in an ion pair to the D260 side chain; the loss of this ion pair at the D260G variant results in a 6.5 kcal/mol increase in $\Delta G^{\ddagger}$ for k_{cat}/K_m for reduction of DHAP.[5] The R269 side chain is immobilized by interactions with the DHAP phosphodianion and the Q295 side chain; Q295 substitutions result in a ≤3.0 kcal/mol increase in $\Delta G^{\ddagger}$ for k_{cat}/K_m for reduction of DHAP.[11] The K204 side chain cation also lies close to the carbonyl group of bound DHAP, but the effect of K204 substitutions on enzyme activity is not yet known.

The determination of kinetic parameters for wild type and variant enzymes over a broad range of pH reports on the effect of changing the ionization state of active site side chains on enzymatic activity.[12−15] For example, the observation of breaks in pH−rate profiles shows the effect of changing side chain protonation or deprotonation on enzyme activity and gives rise to hypotheses for the specific side chains responsible for these breaks. These hypotheses may then be examined by comparing pH−rate profiles for wild type and variant enzymes. We report here the pH−rate profiles for k_{cat}/K_m and k_{cat} for reduction of DHAP by NADH catalyzed by wild type and K120A variant *hl*GPDH, and for k_{cat}/K_dK_{am} for rescue of the K120A variant by $CH_3CH_2NH_3^+$, where K_{am} and K_d are apparent dissociation constants for $CH_3CH_2NH_3^+$ and DHAP, respectively. The effects of the K120A substitution on these pH−rate profiles provide strong evidence for a pH-dependent change in the favored reaction pathway, from a reaction at high pH through a transition state that is stabilized by exogenous ethylammonium cation to a reaction at low pH through a transition state that shows no detectable stabilizing interaction with $CH_3CH_2NH_3^+$, which is governed by protonation of an active site side chain with a pK_a of 5. We propose that protonation of the carboxylate side chain of D260 at the K120A variant provides an acid to substitute for the excised K120 side chain in stabilizing negative charge at O-2 of DHAP, which develops at the hydride transfer transition state. These profiles show that protonation of a second side chain, with $pK_a \approx 8$, is required to observe full activity. We propose that this is the alkyl amine side chain of K204.

EXPERIMENTAL SECTION

The sources of chemical and biochemical reagents and most of the methods for the experiments reported herein were described in a recent publication.[5] This includes the methods for preparation of solutions used in enzyme kinetic studies and for the preparation of the K120A variant of *hl*GPDH. Stock solutions of DHAP were prepared by dissolving the lithium salt of DHAP in water. The pH was adjusted to the desired final pH using 1.0 N NaOH or 1 N HCl, and the concentration of DHAP was determined as the concentration of NADH consumed during quantitative *hl*GPDH-catalyzed reduction. Published procedures were used to prepare stock solutions of the ethylammonium cation,[16] and the pH was adjusted to the desired final pH using 1.0 N NaOH or 1 N HCl. The following reagent grade buffers were purchased from Sigma-Aldrich: sodium acetate, 2-(*N*-morpholino)ethanesulfonic acid (MES), 3-morpholinopropane-1-sulfonic acid (MOPS), triethanolamine·HCl (TEA), [tris(hydroxymethyl)methylamino]-propanesulfonic acid (TAPS), and *N*-cyclohexyl-2-aminoethanesulfonic acid (CHES).

***hl*GPDH-Catalyzed Reduction of DHAP.** The *hl*GPDH-catalyzed reduction of DHAP by NADH was assayed in solutions containing the appropriate buffer (20 mM), 0.1 mg/mL BSA, 200 μM NADH, and 0.04−8 mM DHAP at an ionic strength (I) of 0.12 (NaCl). The following buffers were used for these experiments: acetate buffer, 40% and 60% basic form at pH 4.6 and 4.9, respectively; MES buffer, 15%, 40%, 70%, and 80% basic form at pH 5.4, 6.0, 6.5, and 6.8, respectively; MOPS buffer, 40% and 50% basic form at pH 7.0 and 7.25, respectively; TEA buffer, 30% basic form at pH 7.5; TAPS buffer, 25% and 55% basic form at pH 8.0 and 8.5, respectively; and CHES buffer, 35% basic form at pH 9.0. The initial velocity (v) for the reduction of DHAP was determined from the change in absorbance at 340 nm over a 5−10 min reaction time. The kinetic parameters k_{cat} and K_m for *hl*GPDH-catalyzed reactions were determined from the nonlinear least-squares fit of plots of v/[E] against [DHAP] to the Michaelis−Menten equation (eq 1), where [DHAP] is the concentration of the carbonyl form of DHAP that is present as 55% of total DHAP.[17]

$$\frac{v}{[E]} = \frac{k_{cat}[DHAP]}{K_m + [DHAP]} \quad (1)$$

The K120A variant *hl*GPDH-catalyzed reduction of DHAP by NADH in the presence of $CH_3CH_2NH_3^+$ was monitored in solutions containing 0.1 mg/mL BSA, 200 μM NADH, 0.5−5 mM DHAP, and 20−80 mM $CH_3CH_2NH_3^+$ at I = 0.12 (NaCl),[5,9] and using the same buffers as given above for

https://dx.doi.org/10.1021/acs.biochem.0c00801
Biochemistry 2020, 59, 4856−4863

*hl*GPDH-catalyzed reduction of DHAP in the absence of $CH_3CH_2NH_3^+$. The initial velocity v for the reduction of DHAP was determined from the change in absorbance at 340 nm over a 5−10 min reaction time. The nonlinear least-squares fits of pH−rate profiles to the kinetic equations given in the Discussion were obtained using Prism 8 for MacOS from GraphPad Software.

RESULTS

Wild type and K120A variant *hl*GPDH were prepared by published procedures.[5,18] The initial velocity (v) for *hl*GPDH-catalyzed reduction of DHAP by NADH (200 μM) was determined by monitoring the decrease in absorbance at 340 nm. Figures S1 and S2 show Michaelis−Menten plots of $v/[E]$ against [DHAP] for wild type and K120A variant *hl*GPDH-catalyzed reduction of this substrate by NADH (200 μM), at numerous pH values between 4.6 and 9.0 [I = 0.12 (NaCl)]. The *hl*GPDH-catalyzed reduction of DHAP by NADH is by an ordered reaction mechanism, with NADH (K_d = 7.0 μM)[19,20] binding first.[21,22] Identical (±10%) kinetic parameters k_{cat} and k_{cat}/K_m were previously obtained from Michaelis−Menten plots of $v/[E]$ against [DHAP] for wild type and K120A variant *hl*GPDH-catalyzed reduction of DHAP by 100 and 200 μM NADH at pH 7.5.[5,18] We concluded that these forms of *hl*GPDH are saturated at pH 7.5 for reactions at 100 μM NADH. We show here (Figures S1 and S2) that identical (±10%) values of k_{cat} and k_{cat}/K_m are obtained for wild type and K120A variant *hl*GPDH-catalyzed reduction of DHAP by 100 and 200 μM NADH at the pH extremes of 4.9 and 9.0.

The kinetic parameters k_{cat} and k_{cat}/K_m for *hl*GPDH-catalyzed reactions, determined from the nonlinear least-squares fit of plots of $v/[E]$ against [DHAP] to eq 1, are listed in Table S1. In several cases, we determined separate sets of kinetic parameters at the same pH, but with separately purified preparations of *hl*GPDH. The agreement between kinetic parameters from different batches of enzyme is better than ±10%.

Figure S3 shows plots of $v/[E]$ against $[CH_3CH_2NH_3^+]$, determined at pH 4.9 and 6.0, 25 °C, and I = 0.12 (NaCl), for reduction of DHAP by NADH (200 μM) catalyzed by the K120A variant at several different fixed DHAP concentrations. These plots show that $v/[E]$ is independent of $[CH_3CH_2NH_3^+]$ for reactions at low pH, in contrast to the efficient rescue of the K120A variant observed for reactions at pH 7.5.[5] Figure S4 shows plots of $v/[E]$ against [DHAP] for K120A variant *hl*GPDH-catalyzed reduction of DHAP by NADH (200 μM) at 25 °C, I = 0.12 (NaCl), and different fixed concentrations of $CH_3CH_2NH_3^+$, for reactions at numerous pH values between 6.5 and 9.0. The values of $(k_{cat}/K_m)_{obs} = \frac{k_{cat}[RNH_3^+]}{K_dK_{am}}$ for reactions in the presence of different fixed $CH_3CH_2NH_3^+$ concentrations (Figure S4) were determined as the slopes of linear correlations of $v/[E]$ against [DHAP] for reactions at pH 6.5−9.0 (eq 2, derived for Scheme 2). Values of $\frac{k_{cat}}{K_dK_{am}}$ for activation of the K120A variant by $CH_3CH_2NH_3^+$ were determined as the slopes of plots of $(k_{cat}/K_m)_{obs}$ against $[CH_3CH_2NH_3^+]$. In several cases, we determined values of k_{cat}/K_dK_{am} at a single pH, but with two separately prepared and purified samples of *hl*GPDH. The agreement between kinetic parameters from different batches of the enzyme is better than ±10%.

Scheme 2. Rescue of the Catalytic Activity of K120A *hl*GPDH by $CH_3CH_2NH_3^+$

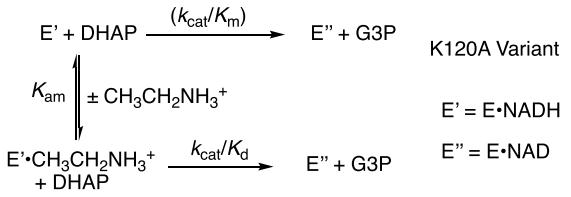

$$\left(\frac{v}{[E]}\right)_{obs} = \left(\frac{v}{[E]}\right)_{o} + \left(\frac{k_{cat}[RNH_3^+][DHAP]}{K_dK_{am}}\right) \quad (2)$$

Figures 2 and 3 show pH−rate profiles constructed using the kinetic parameters k_{cat}/K_m, k_{cat}/K_dK_{am} (Scheme 2), and k_{cat}

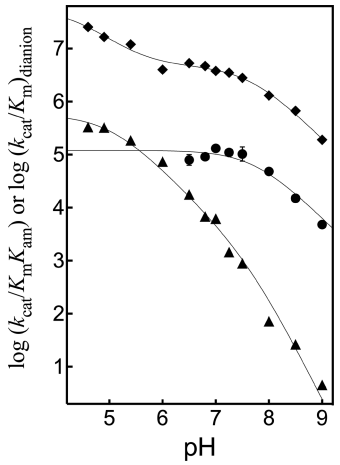

Figure 2. pH profiles of second-order rate constants $(k_{cat}/K_m)_{dianion}$ for the wild type (◆) and K120A variant (▲) *hl*GPDH-catalyzed reduction of the DHAP dianion by NADH and for third-order rate constants (k_{cat}/K_dK_{am}) (●) for rescue of the K120A variant by $CH_3CH_2NH_3^+$ (Scheme 2).

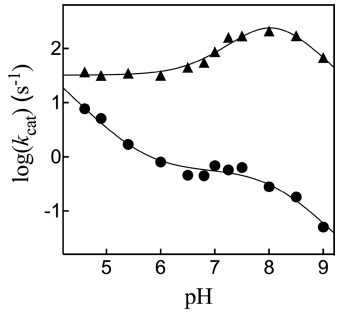

Figure 3. pH profiles of the observed first-order rate constants (k_{cat}) for the wild type (▲) and K120A variant (●) *hl*GPDH-catalyzed reduction of DHAP by NADH.

reported in Table S1. *hl*GPDH shows a high specificity for catalysis of the reaction of the DHAP phosphodianion, compared with the monoanion. This arises from the tight ion pair interaction with the cationic side chain of R269, which is estimated to stabilize the hydride transfer transition state by 9 kcal/mol.[8,9,23] The values of $(k_{cat}/K_m)_{dianion}$ reported in Figure 2 are calculated from $(k_{cat}/K_m)_{obs}$ (Table S1) as (k_{cat}/

https://dx.doi.org/10.1021/acs.biochem.0c00801
Biochemistry 2020, 59, 4856−4863

$K_m)_{dianion}$ = $(k_{cat}/K_m)_{obs}/f_{dianion}$, where $f_{dianion}$ is determined from the reaction pH and a pK_a of 6.0 for ionization of the DHAP monoanion to form the dianion.[24] Figure 2 also shows the pH profiles for second-order rate constants $(k_{cat}/K_m)_{dianion}$ for K120A *hl*GPDH-catalyzed reduction of DHAP by NADH, and the observed third-order rate constants $(k_{cat}/K_dK_{am})_{obs}$ for activation of the K120A variant by $CH_3CH_2NH_3^+$. Figure 3 shows the pH profiles for observed first-order rate constants $(k_{cat})_{obs}$ for wild type and K120A *hl*GPDH-catalyzed reduction of DHAP by NADH. The uncertainty in these kinetic parameters, estimated as the average of values determined in separate experiments and using different batches of enzyme, is generally smaller than the symbol in the figure: the exception is data for rescue of the activity of the K120A variant by $CH_3CH_2NH_3^+$ [Figure 2 (●)].

DISCUSSION

We note the following unusual features of the pH−rate profiles for the kinetic parameters k_{cat}/K_m and k_{cat}/K_dK_{am} (Figure 2) and k_{cat} (Figure 3).

(1) In three of four pH profiles for k_{cat}/K_m and k_{cat} for wild type and K120A variant GPDH, the kinetic parameter is observed to increase at low pH, in contrast to the expected pH optima at physiological neutral pH. The exception is the profile for values of k_{cat} for the wild type enzyme, but these values show an only 7-fold change as the pH is decreased from 9.0 to 4.6, and a maximum at pH 8.

(2) A value of $(\Delta\log k_{cat}/K_m)/(\Delta pH) = \{\log[(840\ M^{-1}\ s^{-1})/(4.7\ M^{-1}\ s^{-1})]/1.5\} = 1.5$ can be calculated from data for K120A *hl*GPDH-catalyzed reactions of DHAP at pH 9.0 and 7.5 (Figure 2). This is consistent with a slope of >1.0 over this pH range and with the requirement for addition of more than one proton to the K120A variant as the pH is changed from pH 9 to 6, and the variant *hl*GPDH is converted to the catalytically active form (see below for the fit of these data from Figure 2).

(3) The pH−rate profiles from Figure 2 show increasing values of $\log(k_{cat}/K_m)_{dianion}$ for the K120A variant-catalyzed reduction of DHAP, with a decrease in pH, relative to the pH-independent values of $\log(k_{cat}/K_dK_{am})$ for the rescue of this variant by $CH_3CH_2NH_3^+$. At pH <6.5, where $(k_{cat}/K_m)_{dianion} \gg (k_{cat}/K_dK_{am})[CH_3CH_2NH_3^+]$, rescue is no longer detected. These results require a change, with the changing protonation state of *hl*GPDH, in the dominant pathway for the K120A variant-catalyzed reduction of DHAP, from a hydride transfer reaction at high pH through a transition state stabilized by exogenous $CH_3CH_2NH_3^+$, to a reaction at pH ≤6.5 through a transition state that shows no detectable stabilization by this cation.

Modeling the pH−Rate Profiles. We speculate about the identity of the catalytic side chains that give rise to the breaks in the pH−rate profiles shown in Figures 2 and 3 but focus on the qualitative insight that these profiles provide into the roles of these side chains in stabilization of the hydride transfer transition state. Figure 2 shows the fit of the values of $\log(k_{cat}/K_dK_{am})$ to eq 2, derived for Scheme 3 for the rescue of the variant by $CH_3CH_2NH_3^+$, using the following values: pK_b = 7.7 and $k_{cat}/K_dK_{am} = (1.2 \pm 0.17) \times 10^5\ M^{-2}\ s^{-1}$. By comparison, a k_{cat}/K_dK_{am} value of $0.85 \times 10^5\ M^{-2}\ s^{-1}$ was reported in an earlier study at pH 7.5.[5] We propose that a pK_b of 7.7 is for deprotonation of the K204 side chain cation, which lies close to the bound substrate (Figure 1).

Scheme 3. Kinetic Scheme for Activation of K120A *hl*GPDH Used to Rationalize the pH Profile for Values of k_{cat}/K_dK_{am} (●) Shown in Figure 2 for the Rescue of the K120A Variant by $CH_3CH_2NH_3^+$

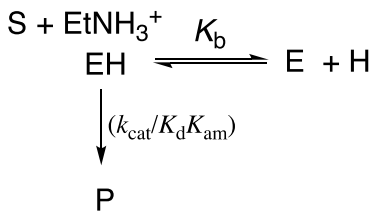

$$(k_{cat}/K_mK_d)_{obs} = (k_{cat}/K_dK_{am})\left(\frac{[H^+]}{K_b + [H^+]}\right) \quad (2)$$

The pH−rate profiles for $\log(k_{cat}/K_m)_{dianion}$ (Figure 2) and $\log k_{cat}$ (Figure 3) were fit to equations derived for Schemes 4,

Scheme 4. Kinetic Schemes for *hl*GPDH-Catalyzed Reduction of DHAP[a]

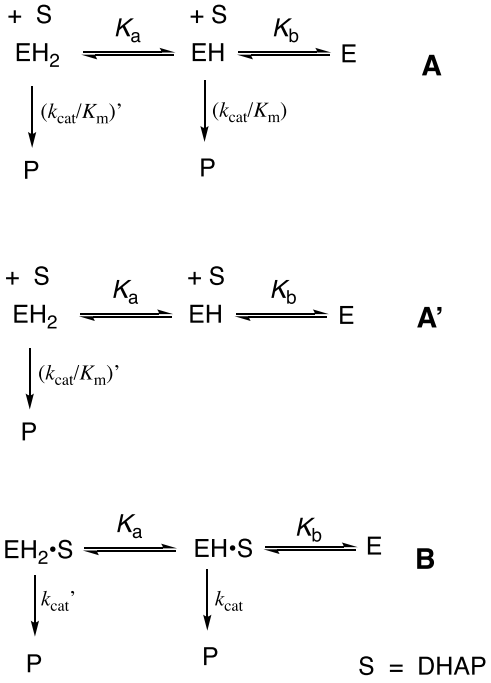

[a]A and A′ were used to rationalize the pH−rate profiles for $(k_{cat}/K_m)_{dianion}$ (Figure 2); B was used to rationalize the pH−rate profiles for k_{cat} (Figure 3).

in which *hl*GPDH exists largely in the inactive form E at high pH and is converted to EH and EH_2 by protonation of side chains with pK_b and pK_a, respectively. Figure 2 shows the nonlinear least-squares fit of values of $\log(k_{cat}/K_m)_{dianion}$ to eq 3, derived for Scheme 4A, for reactions catalyzed by wild type *hl*GPDH. This fit gives the following values: pK_a ≈ 4.4, pK_b = 7.6, $(k_{cat}/K_m)' = 5.7 \times 10^7\ M^{-1}\ s^{-1}$, and $(k_{cat}/K_m) = 4.7 \times 10^6\ M^{-1}\ s^{-1}$. We propose that a p$K_b$ of 7.6 is for deprotonation of the K204 side chain cation and exclude the K120 side chain for pK_b, because a similar downward break is observed for the pH profile for values of k_{cat}/K_dK_{am} for the K120A variant. The poorly defined break in the profile for $(k_{cat}/K_m)_{dianion}$ observed at low pH is due to either (1) protonation of an essential side

https://dx.doi.org/10.1021/acs.biochem.0c00801
Biochemistry 2020, 59, 4856−4863

chain with a pK_a of ≈4.4 or (2) a change in the rate-determining step for the enzyme-catalyzed hydride transfer, from reduction of DHAP to rate-determining formation of the Michaelis complex to DHAP. The value of $(k_{cat}/K_m)'$ of 5.7×10^7 M^{-1} s^{-1} obtained from this fit lies within the range of values for second-order rate constants determined for rate-determining substrate binding in other enzymatic reactions.[25,26]

$$(k_{cat}/K_m)_{dianion} = (k_{cat}/K_m)'\left(\frac{1}{1 + \frac{K_a}{[H^+]} + \frac{K_aK_b}{[H^+]^2}}\right) + (k_{cat}/K_m)\left(\frac{1}{1 + \frac{[H^+]}{K_a} + \frac{K_b}{[H^+]}}\right) \quad (3)$$

$$(k_{cat}/K_m)_{dianion} = (k_{cat}/K_m)'\left(\frac{1}{1 + \frac{K_a}{[H^+]} + \frac{K_aK_b}{[H^+]^2}}\right) \quad (3')$$

$$(k_{cat})_{obs} = (k_{cat})'\left(\frac{1}{1 + \frac{K_a}{[H^+]} + \frac{K_aK_b}{[H^+]^2}}\right) + k_{cat}\left(\frac{1}{1 + \frac{[H^+]}{K_a} + \frac{K_b}{[H^+]}}\right) \quad (4)$$

$$(k_{cat})_{obs} = (k_{cat})'[H^+]/K_a + k_{cat}\left(\frac{1}{1 + \frac{[H^+]}{K_a} + \frac{K_b}{[H^+]}}\right) \quad (4')$$

The fit of the values of $\log(k_{cat}/K_m)_{dianion}$ to eq 3′, derived for Scheme 4A′, for reactions catalyzed by the K120A variant of *hl*GPDH is shown in Figure 2, where EH shows no detectable activity toward catalysis of reduction of DHAP. The theoretical line through these data was drawn for the following values: pK_a = 5.0, pK_b = 7.6, and $(k_{cat}/K_m)'$ = 5.6×10^5 M^{-1} s^{-1}. The pK_b value of 7.6 is in good agreement with the pK_b of 7.7 determined from the fit of the data for the rescue of the K120A variant by $CH_3CH_2NH_3^+$ (Scheme 3). This is required because the unactivated and $CH_3CH_2NH_3^+$-activated reactions of K120A variant DHAP involve monoprotonated *hl*GPDH [EH (Schemes 3 and 4A′)]. We propose that the pK_b of 7.6 is for the K204 side chain cation and that the pK_a of 5.0 is for protonation of the D260 side chain to form EH_2, which is discussed below.

Figure 3 shows the fit to eq 4, derived for Scheme 4B, of values of log k_{cat} for the reaction catalyzed by wild type *hl*GPDH. This fit gives the following values: pK_b = 8.1, pK_a = 8.0, k_{cat} = 720 s^{-1}, and k_{cat}' = 32 s^{-1}. Figure 3 shows that the Michaelis complex of DHAP with wild type *hl*GPDH maintains robust catalytic activity throughout the entire pH range. The pH maximum is more hump- than bell-shaped, because only small decreases in log k_{cat} were observed on both sides of the maximum. These data may also be fit by co-dependent values of pK_a, pK_b, k_{cat}, and k_{cat}' for a "reverse protonation" reaction mechanism,[27] where the essential proton at the monoprotonated enzyme sits at the less basic of two ionizable side chains (pK_a > pK_b), so that the active enzyme EH·S (Scheme 4B) is never the major form. We are unable to rigorously exclude "reverse protonation" for the reaction of these side chains but propose a relatively simple model in which (1) the pK_b of 8.1 is for deprotonation of the K204 side chain, which gives a functional active site, (2) the K120 side chain, which is stabilized by an ion pair to D260, remains protonated throughout the entire pH range for Figure 3, and (3) there is a third unidentified side chain that provides a modest stabilization of the hydride transfer transition state when protonated. This could be one of several second-shell ionizable active site side chains.

Figure 3 shows the fit of values of log k_{cat} to eq 4′, derived for Scheme 4B, where $K_a \gg [H^+]$, for the reaction catalyzed by the K120A variant of *hl*GPDH. This fit gives the following values: pK_b = 8.1, k_{cat} = 0.57 s^{-1}, and k_{cat}'/K_a = 2.9×10^5 M^{-1} s^{-1}. We propose that the pK_b of 8.1 is for deprotonation of the K204 side chain. We suggest that the pK_a of <4.6 is for the carboxylic acid side chain of D260, and that this side chain substitutes for the cationic K120 side chain for the variant-catalyzed hydride transfer reaction at low pH.

Enzymatic Reaction Mechanism. Three ionizable amino acid side chains lie close to DHAP bound to wild type *hl*GPDH (Figure 1); K120, K204, and D260 (Scheme 5). We have proposed that the K120 side chain cation acts to stabilize negative charge at the C-2 oxygen, which develops at the hydride transfer transition state, and have provided support for this proposal in studies of the K120A variant.[5,9] The pH−rate profiles from Figure 2 [$(k_{cat}/K_m)_{dianion}$] and Figure 3 (k_{cat}) for wild type *hl*GPDH show that this enzyme is activated by protonation of a side chain with a pK_a of 7.6−8.0. This side chain is not K120, because the pH−rate profiles for the K120A variant from Figure 2 (k_{cat}/K_dK_{am}) and Figure 3 (k_{cat}) show the same requirement for a protonated side chain with a pK_a of 8.0.

Scheme 5 provides a rationalization for the pH profiles for $(k_{cat}/K_m)_{dianion}$ (Figure 2) for reactions catalyzed by wild type *hl*GPDH. (1) The side chain cation of K120 is stabilized by an ion pair to the D260 side chain anion and remains protonated from pH 4.6 to 9.0. This ion pair is required for efficient catalysis of hydride transfer, as shown by the observation that the D260G substitution results in a large 60000-fold decrease in k_{cat}/K_m for reduction of DHAP. (2) Protonation of K204 at

Scheme 5. Assignments of Basic Amino Acid Side Chains Whose Protonation States Are Proposed to Control the pH−Rate Profiles Shown in Figures 2 and 3

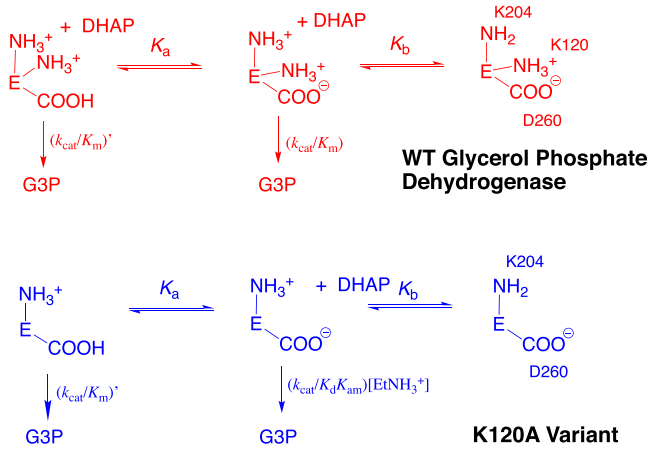

https://dx.doi.org/10.1021/acs.biochem.0c00801
Biochemistry 2020, 59, 4856−4863

Scheme 6. Hypothetical GPDH-Catalyzed Hydride Transfer from NADH to DHAP to Form an Alkoxide Anion Intermediate Stabilized by the K120 and K204 Side Chain Cations[a]

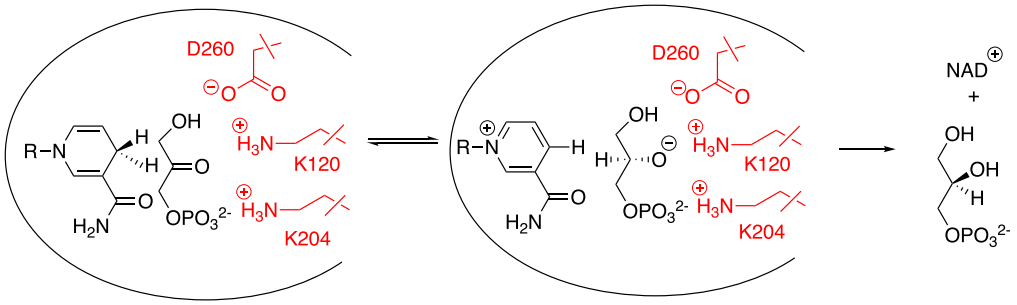

[a]The second step of proton transfer forming neutral and enzyme-bound G3P is not shown.

wild type *hl*GPDH, with a pK_b of 7.6, provides additional electrostatic stabilization of the hydride transfer transition state. (3) Protonation of D260, with a pK of ≤4.6, activates the enzyme for catalysis of reduction of DHAP, perhaps by enhancing transition state stabilization from the neighboring K120 side chain.

The pH profile for $(k_{cat}/K_m)_{dianion}$ for the K120A variant (Figure 2) shows that two protons, with pK_b and pK_a values of 7.6 and 5.0, respectively, must be added to variant side chains at pH 9 to form a protein catalyst that is active toward reduction of DHAP. This requires that $(k_{cat}/K_m)' \gg (k_{cat}/K_m)$ for Scheme 5. By contrast, addition of only a single proton is sufficient to give an enzyme that is activated for catalysis by exogenous $CH_3CH_2NH_3^+$, the analogue of the excised K120 side chain. We conclude that different forms of *hl*GPDH catalyze the $CH_3CH_2NH_3^+$-activated and unactivated reduction of DHAP by NADH and propose that the protonated D260 side chain (Scheme 5), with a pK_a of 5.0, acts at low pH in place of the excised K120 side chain. The latter proposal is consistent with the results of a recent computational study that modeled the effects of a K120A substitution in *hl*GPDH on enzyme activity.[28]

The large differences in the pH profiles for $\log(k_{cat}/K_m)_{dianion}$ (Figure 2) and $\log k_{cat}$ (Figure 3) for the wild type and K120A variant are attributed to the effects of the phosphodianion-driven enzyme conformational change[3,5] on the function of active site side chains. In the case of the K120A variant, the dianion-driven closure of an active site loop over DHAP results in a change from sharply changing values of $\log(k_{cat}/K_m)_{dianion}$ at neutral pH (Figure 2) to a plateau in the profile for $\log k_{cat}$ (Figure 3) for catalysis by the monoprotonated form of *hl*GPDH [EH (Scheme 4B)]. This shows that side chain reorganization, which accompanies the enzyme conformational change, promotes catalysis of hydride transfer by the monoprotonated K120A variant enzyme at neutral pH due, at least in part, to an enhancement of transition state stabilization by the cationic K204 side chain.

The pH profile for $\log(k_{cat}/K_m)_{dianion}$ for wild type *hl*GPDH (Figure 2) shows a downward break centered at pH 7.6. By contrast, there is a hump in the profile for $\log k_{cat}$ (Figure 3) that is consistent with an ∼20-fold increase in enzyme reactivity as the pH is increased from 6.0 [$k_{cat}' = 32\ s^{-1}$ (Scheme 4B)] to 8.0 [$k_{cat} = 720\ s^{-1}$ (Scheme 4B)]. This hump shows that the phosphodianion-driven enzyme conformational change promotes ionization of an unidentified side chain, which results in a 7-fold increase in k_{cat} for reduction of enzyme-bound DHAP (Figure 3).

Brønsted Catalysis at the Carbonyl Oxygen. The Nε atom of K120 is nearly in the plane defined by the trigonal C═O bond of DHAP bound to *hl*GPDH (Figure 1). It is well-positioned to protonate this oxygen, while the Nε atom of K204 lies well below this plane and was judged to be less likely to participate directly in protonation of the carbonyl oxygen.[5] Our results are consistent with a model in which protonated side chains of K120 and K204 act together in the stabilization of the transition state for *hl*GPDH-catalyzed hydride transfer. The proximity of these two cationic side chains to O-2 favors a "late" transition state, with the nearly complete hydride transfer to the carbonyl carbon providing for optimal stabilizing electrostatic interactions between the side chain cations and negative charge at O-2. There are at least two advantages for the fully stepwise pathway shown in Scheme 6, where the transfer of a hydride to carbon and the transfer of a proton to oxygen occur as separate steps.

(1) Immobilization of the K120 side chain in an ion pair with D260 provides for the unusually efficient electrostatic rescue of the K120A variant by $CH_3CH_2NH_3^+$.[9] By comparison, the formation of the stable K120-D260 ion pair should result in a decrease in the acidity of the K120 side chain, or the rescue agent, for deprotonation to form an amine that eliminates the stable ion pair. This decrease in acidity will reduce the driving force for a concerted hydride transfer reaction mechanism, where there is formal proton transfer from either the K120 side chain or $CH_3CH_2NH_3^+$ rescue agent to O-2 of DHAP.

(2) Any transition state stabilization obtained from the concerted transfer of a proton to the developing O-2 oxyanion will be balanced by a weakening of stabilizing electrostatic interactions with the K120 and K204 side chains, which accompanies neutralization of negative charge from proton transfer to O-2. We suggest that the stepwise pathway, with no formal proton transfer to oxygen, provides for optimal electrostatic interactions between the protein catalyst and reaction transition state.[29,30]

The robust activity for the K120A variant at low pH (Figures 2 and 3) is rationalized by the recruitment of the neutral protonated D260 side chain, to serve in place of cationic K120, in stabilization of negative charge at O-2 at the hydride transfer transition state. This is consistent with a plasticity in side chain function at the active site of *hl*GPDH. We suggest that the change in the side chain that participates in protonation of O-2 from the weakly acidic and cationic K120 side chain for wild type *hl*GPDH to the strongly acidic and neutral protonated D260 of the K120A variant might be accompanied by a change

https://dx.doi.org/10.1021/acs.biochem.0c00801
Biochemistry 2020, 59, 4856−4863

to a concerted reaction mechanism due to the increase in the driving force for protonation of O-2 by the acidic D260 side chain.

■ ASSOCIATED CONTENT

Supporting Information

The Supporting Information is available free of charge at https://pubs.acs.org/doi/10.1021/acs.biochem.0c00801.

Kinetic parameters k_{cat} and $(k_{cat}/K_m)_{obs}$, $(k_{cat}/K_m)_{dianion}$, and k_{cat}/K_dK_{am} for wild type and K120A variant *hl*GPDH reactions, respectively (Table S1); Michaelis−Menten plots for wild type and the K120A variant *hl*GPDH-catalyzed reduction of DHAP by NADH at pH 4.6−9.0 (Figures S1 and S2, respectively); effect of increasing concentrations of $CH_3CH_2NH_3^+$ on $v/[E]$ for K120A variant *hl*GPDH-catalyzed reduction of DHAP, determined at several different fixed concentrations of DHAP at pH 4.9 and 6.0 (Figure S3); effect of increasing concentrations of DHAP on $v/[E]$ for K120A variant *hl*GPDH-catalyzed reduction of DHAP determined at several different fixed concentrations of $CH_3CH_2NH_3^+$ at pH 6.5−9.0 (Figure S4A); and effect of increasing concentrations of $CH_3CH_2NH_3^+$ on the apparent second-order rate constant for K120A *hl*GPDH-catalyzed reduction of DHAP determined at pH 6.5−9.0 (Figure S4B) (PDF)

Accession Codes

Human glycerol-3-phosphate dehydrogenase [NAD(+)], cytoplasmic, P21695.

■ AUTHOR INFORMATION

Corresponding Author

John P. Richard − *Department of Chemistry, University at Buffalo, The State University of New York at Buffalo, Buffalo, New York 14260-3000, United States;* orcid.org/0000-0002-0440-2387; Email: jrichard@buffalo.edu

Authors

Rui He − *Department of Chemistry, University at Buffalo, The State University of New York at Buffalo, Buffalo, New York 14260-3000, United States*

Judith R. Cristobal − *Department of Chemistry, University at Buffalo, The State University of New York at Buffalo, Buffalo, New York 14260-3000, United States*

Naiji Jabin Gong − *Department of Chemistry, University at Buffalo, The State University of New York at Buffalo, Buffalo, New York 14260-3000, United States*

Complete contact information is available at: https://pubs.acs.org/10.1021/acs.biochem.0c00801

Funding

The authors acknowledge National Institutes of Health Grants GM116921 and GM134881 for generous support of this work.

Notes

The authors declare no competing financial interest.

■ ABBREVIATIONS

GPDH, glycerol-3-phosphate dehydrogenase; *hl*GPDH, glycerol-3-phosphate dehydrogenase from human liver; DHAP, dihydroxyacetone phosphate; NADH, nicotinamide adenine dinucleotide, reduced form; NAD, nicotinamide adenine dinucleotide, oxidized form; MES, 2-(*N*-morpholino)-ethanesulfonic acid; MOPS, 3-morpholinopropane-1-sulfonic acid; TEA, triethanolamine; TAPS, [tris(hydroxymethyl)-methylamino]propanesulfonic acid; CHES, *N*-cyclohexyl-2-aminoethanesulfonic acid; BSA, bovine serum albumin.

■ REFERENCES

(1) Fondy, T. P., Levin, L., Sollohub, S. J., and Ross, C. R. (1968) Structural Studies on Nicotinamide Adenine Dinucleotide-linked l-Glycerol 3-Phosphate Dehydrogenase Crystallized from Rat Skeletal Muscle. *J. Biol. Chem. 243*, 3148−3160.

(2) Tsang, W.-Y., Amyes, T. L., and Richard, J. P. (2008) A Substrate in Pieces: Allosteric Activation of Glycerol 3-Phosphate Dehydrogenase (NAD^+) by Phosphite Dianion. *Biochemistry 47*, 4575−4582.

(3) Ou, X., Ji, C., Han, X., Zhao, X., Li, X., Mao, Y., Wong, L.-L., Bartlam, M., and Rao, Z. (2006) Crystal structures of human glycerol 3-phosphate dehydrogenase 1 (GPD1). *J. Mol. Biol. 357*, 858−869.

(4) Richard, J. P. (2019) Protein Flexibility and Stiffness Enable Efficient Enzymatic Catalysis. *J. Am. Chem. Soc. 141*, 3320−3331.

(5) Mydy, L. S., Cristobal, J., Katigbak, R., Bauer, P., Reyes, A. C., Kamerlin, S. C. L., Richard, J. P., and Gulick, A. M. (2019) Human Glycerol 3-Phosphate Dehydrogenase: X-Ray Crystal Structures that Guide the Interpretation of Mutagenesis Studies. *Biochemistry 58*, 1061−1073.

(6) Richard, J. P., Amyes, T. L., Goryanova, B., and Zhai, X. (2014) Enzyme architecture: on the importance of being in a protein cage. *Curr. Opin. Chem. Biol. 21*, 1−10.

(7) Choe, J., Guerra, D., Michels, P. A. M., and Hol, W. G. J. (2003) Leishmania mexicana glycerol-3-phosphate dehydrogenase showed conformational changes upon binding a bi-substrate adduct. *J. Mol. Biol. 329*, 335−349.

(8) Reyes, A. C., Koudelka, A. P., Amyes, T. L., and Richard, J. P. (2015) Enzyme Architecture: Optimization of Transition State Stabilization from a Cation−Phosphodianion Pair. *J. Am. Chem. Soc. 137*, 5312−5315.

(9) Cristobal, J. R., Reyes, A. C., and Richard, J. P. (2020) The Organization of Active Site Side Chains of Glycerol-3-phosphate Dehydrogenase Promotes Efficient Enzyme Catalysis and Rescue of Variant Enzymes. *Biochemistry 59*, 1582−1591.

(10) Reyes, A. C., Amyes, T. L., and Richard, J. P. (2016) Enzyme Architecture: A Startling Role for Asn270 in Glycerol 3-Phosphate Dehydrogenase-Catalyzed Hydride Transfer. *Biochemistry 55*, 1429−1432.

(11) He, R., Reyes, A. C., Amyes, T. L., and Richard, J. P. (2018) Enzyme Architecture: The Role of a Flexible Loop in Activation of Glycerol-3-phosphate Dehydrogenase for Catalysis of Hydride Transfer. *Biochemistry 57*, 3227−3236.

(12) Karsten, W. E., and Cook, P. F. (2006) Substrate and pH dependence of isotope effects in enzyme catalyzed reactions. In *Isotope Effects in Chemistry and Biology* (Kohen, A., and Limbach, H.-H., Eds.) pp 793−809, CRC Press LLC, Boca Raton, FL.

(13) Khavrutskii, I. V., Compton, J. R., Jurkouich, K. M., and Legler, P. M. (2019) Paired Carboxylic Acids in Enzymes and Their Role in Selective Substrate Binding, Catalysis, and Unusually Shifted pK_a Values. *Biochemistry 58*, 5351−5365.

(14) Grimshaw, C. E., Cook, P. F., and Cleland, W. W. (1981) Use of isotope effects and pH studies to determine the chemical mechanism of Bacillus subtilis L-alanine dehydrogenase. *Biochemistry 20*, 5655−5661.

(15) Viola, R. E., and Cleland, W. W. (1978) Use of pH studies to elucidate the chemical mechanism of yeast hexokinase. *Biochemistry 17*, 4111−4117.

(16) Go, M. K., Amyes, T. L., and Richard, J. P. (2010) Rescue of K12G mutant TIM by NH_4^+ and alkylammonium cations: The reaction of an enzyme in pieces. *J. Am. Chem. Soc. 132*, 13525−13532.

(17) Reynolds, S. J., Yates, D. W., and Pogson, C. I. (1971) Dihydroxyacetone phosphate. Its structure and reactivity with α-glycerolphosphate dehdyrogenase, aldolase and triose phosphate

isomerase and some possible metabolic implications. *Biochem. J. 122*, 285−297.
(18) Reyes, A. C., Zhai, X., Morgan, K. T., Reinhardt, C. J., Amyes, T. L., and Richard, J. P. (2015) The Activating Oxydianion Binding Domain for Enzyme-Catalyzed Proton Transfer, Hydride Transfer and Decarboxylation: Specificity and Enzyme Architecture. *J. Am. Chem. Soc. 137*, 1372−1382.
(19) Reyes, A. C., Amyes, T. L., and Richard, J. P. (2018) Primary Deuterium Kinetic Isotope Effects: A Probe for the Origin of the Rate Acceleration for Hydride Transfer Catalyzed by Glycerol-3-Phosphate Dehydrogenase. *Biochemistry 57*, 4338−4348.
(20) Reyes, A. C. (2016) Enzyme Architecture: Insights into Protein-Phosphodianion Interactions in Glycerol Phosphate Dehydrogenase-Catalyzed Hydride Transfer. Ph.D. Thesis, University at Buffalo, The State University of New York at Buffalo, Buffalo, NY.
(21) Bentley, P., and Dickinson, F. M. (1974) A study of the kinetics and mechanism of rabbit muscle L-glycerol 3-phosphate dehydrogenase. *Biochem. J. 143*, 19−27.
(22) Black, W. J. (1966) Kinetic studies on the mechanism of cytoplasmic L-α-glycerophosphate dehydrogenase of rabbit skeletal muscle, Can. *Can. J. Biochem. 44*, 1301−1317.
(23) Reyes, A. C., Amyes, T. L., and Richard, J. P. (2016) Enzyme Architecture: Self-Assembly of Enzyme and Substrate Pieces of Glycerol-3-Phosphate Dehydrogenase into a Robust Catalyst of Hydride Transfer. *J. Am. Chem. Soc. 138*, 15251−15259.
(24) Plaut, B., and Knowles, J. R. (1972) pH-Dependence of the triosephosphate isomerase reaction. *Biochem. J. 129*, 311−320.
(25) Gadda, G., and Sobrado, P. (2018) Kinetic Solvent Viscosity Effects as Probes for Studying the Mechanisms of Enzyme Action. *Biochemistry 57*, 3445−3453.
(26) Snider, M. G., Temple, B. S., and Wolfenden, R. (2004) The path to the transition state in enzyme reactions: a survey of catalytic efficiencies. *J. Phys. Org. Chem. 17*, 586−591.
(27) Sims, P. A., Larsen, T. M., Poyner, R. R., Cleland, W. W., and Reed, G. H. (2003) Reverse Protonation Is the Key to General Acid−Base Catalysis in Enolase. *Biochemistry 42*, 8298−8306.
(28) Mhashal, A. R., Romero-Rivera, A., Mydy, L. S., Cristobal, J. R., Gulick, A. M., Richard, J. P., and Kamerlin, S. C. L. (2020) Modeling the Role of a Flexible Loop and Active Site Side Chains in Hydride Transfer Catalyzed by Glycerol-3-phosphate Dehydrogenase. *ACS Catal. 10*, 11253−11267.
(29) Kamerlin, S. C. L., Sharma, P. K., Chu, Z. T., and Warshel, A. (2010) Ketosteroid isomerase provides further support for the idea that enzymes work by electrostatic preorganization. *Proc. Natl. Acad. Sci. U. S. A. 107*, 4075−4080.
(30) Warshel, A., Sharma, P. K., Kato, M., Xiang, Y., Liu, H., and Olsson, M. H. M. (2006) Electrostatic basis for enzyme catalysis. *Chem. Rev. 106*, 3210−3235.

https://dx.doi.org/10.1021/acs.biochem.0c00801
Biochemistry 2020, 59, 4856−4863